PCCP

Accepted Manuscript

ROYAL SOCIETY OF CHEMISTRY

www.rsc.org/pccp

A direct Fe-O coordination at FePc/MoO_x interface investigated by XPS and NEXAFS spectroscopies

Lingyun Liu[a], Wenhua Zhang[a*], Panpan Guo[a], Kai Wang[a], Jiaou Wang[b], Haijie Qian[b], Ibrahim Kurash[b], Chia-Hsin Wang[c], Yaw-Wen Yang[c], and Faqiang Xu[a*]

[a]*National Synchrotron Radiation Laboratory, University of Science and Technology of China, Hefei, Anhui 230029, P.R.China*

[b]*Beijing Synchrotron Radiation Laboratory, Institute of High Energy Physics, Chinese Academy of Sciences, Beijing 100039, P.R.China*

[c]*National Synchrotron Radiation Research Center, Hsinchu, 30076, Taiwan*

[*] Corresponding authors: Tel.: +86 55163602060 (Zhang), +86 551 63602127 (Xu); Fax.: +86 551 5141078 (Xu)

E-mail: zhangwh@ustc.edu.cn (Zhang), fqxu@ustc.edu.cn (Xu).

Abstract

Molecule-substrate interaction plays a vital role on the electronic structures and charge transfer properties in organic-transition metal oxides (TMOs) hybridized devices. In this work, the interactions at the FePc/MoO_3 interface has been investigated in detail by using the synchrotron radiation photoemission spectroscopy (SRPES) and the near-edge x-ray absorption fine structure (NEXAFS) spectroscopy. Compared with the annealing of bare MoO_3 film, the FePc adsorption is found to promote the thermal reduction of the underlying MoO_3 film. XPS and NEXAFS experimental results unanimously demonstrate a strong electronic coupling between FePc molecules and the MoO_x ($x < 3$) substrate. A direct Fe-O coordination at the interface as well as an electron transfer from the molecule toward the substrate is proposed. This strong coupling is compatible with the facile electron transfer from FePc molecules toward electrode through a MoO_x interlayer. The understanding of the molecule-substrate interaction at the atomic level is of significance in engineering functionalized surfaces with potential applications in nanoscience, molecular electronics and photonics.

Introduction

In recent years, transition metal oxides (TMOs) have been increasingly employed as the anode buffer layers to achieve facile control of hole transfer and carriers balance in the fabrication of various organic optoelectronic devices[1-6]. It has been found that the hybridization of TMOs with functional organic molecules enables

enhanced charge transfer property at the organic/TMO interface[2-6]. Also, the atomic morphologies and electronic structures of the interface play important roles on the ultimate optical or electric performance of the device. For instance, the interfacial energy level alignment determines energetically the charge transfer dynamics across the interfaces[7, 8], and the chemical interactions influence significantly the interface stabilities[9, 10], including the interfacial diffusion and phase segregations. In addition, the interfacial reactions between the functional organic molecules and the contact TMOs could give rise to new electronic states in the TMO band gap, which may act as electronic level ladders in the band gap and change essentially the properties and functions of the TMO/organic interface[11]. Therefore, a comprehensive understanding of the organic/TMO interface including the electronics structures and the interaction details is urgently needed to better optimize the constructions and thus further improve the performance of relevant devices.

Molybdenum trioxide (MoO_3) has attracted considerable interests as an efficient buffer layer for hole transport due to its high work function (WF = 6.8 eV) and deep-lying conduction band (CB)[1, 12]. The efficient hole injection from electrode can proceed via electron extraction from the highest occupied molecular orbital (HOMO) of the contacting organic layer across the low-lying CB of MoO_3[1]. In addition, the partial reduced MoO_x ($x < 3$) rather than stoichiometric MoO_3 was found to be better for the charge exchange at the OSCs/MoO_x interfaces, thus improve greatly the device performance[13]. For instance, Sun *et al.* studied bulk heterojunction polymer solar cells fabricated with the photoactive layer of PCDTBT:$PC_{70}BM$ and the MoO_x buffer layer

at the anode[13]. Thanks to the long-term air stability of MoO_x, and the efficient charge exchange between the polymer and electrodes, they gained a power conversion up to 7.2%. In contrast to the implementation of MoO_3 for the improvement of relevant devices, however, investigations on the electronic structures and chemical interactions on the atomic level at the OSC/MoO_3 interface are limited. In a previous work, we studied the energy level alignment at the FePc/MoO_x/ITO interface and evidenced that the partially reduced MoO_3 layer was more favorable for hole injection at the interface[12]. Whereas, the interactions between the FePc molecules and the MoO_x substrate is not clear enough. It is known that the chemical interplay between TMOs and the anchored dye molecules vigorously influence the molecular orientation and interfacial electronic structures[14]. Thus the microscopic mechanism of the interaction would be helpful for understanding the electronic properties and charge transfer process at the OSC/MoO_3 interface.

In this work, we will investigate the interactions between a single layer of iron phthalocyanine (FePc) molecules and the partially reduced MoO_3 layer by means of the synchrotron radiation photoemission spectroscopy (SRPES) and near-edge x-ray absorption fine structure (NEXAFS) spectroscopy. Through investigation of the electronic structures and the recognition of the surface species, the core level photoemission spectroscopy is a powerful and direct technique to unravel the chemical reactions and the charge transfer nature that occurring on surface[15-17]. NEXAFS spectroscopy is a very sensitive tool to probe the distribution and symmetries of unoccupied electronic states which are intimately involved in a

chemical reaction or a charge transfer process[18]. FePc is a typical planar molecule with high chemical and thermal stability, and performs as a p-type organic semiconductor with widespread applications in organic devices[19-22]. The thermal desorption of FePc multilayer films on the MoO_x surface leads to an unexpected strong electronic coupling between the FePc molecules and the MoO_x substrate.

Experimental Details

The ITO glass (MTI Co., China) was ultrasonically cleaned in alcohol for 15 minutes. MoO_3 (≥ 99.9%) and FePc (≥ 95%) powders were purchased from the Strem Chemicals, Inc. and the Tokyo Kasei Kogyo Co., Ltd., respectively. 3 nm MoO_3 and multilayer of FePc were successively deposited onto the ITO substrate in a molecular beam epitaxial (MBE) system (CreaTec Fisher & Co. Gmbh). The film thickness was detected by the quartz crystal monitor. The base pressure of the deposition chamber was better than 5×10^{-9} mbar. The 3nm MoO_3 film was reduced via thermal annealing at 400 ℃ for 40 minutes prior to the deposition of FePc film. FePc was deposited at 380 ℃ from a Knuson cell with the substrate keeping at room temperature. The single layer of FePc was gained from the stepwise desorption of the multilayer FePc film at temperature from 100 ℃ to 400 ℃, In this temperature range, the FePc molecules will not decompose [23, 24].

The SRPES experiments were carried out at the 4B9B beamline in the Beijing Synchrotron Radiation Facility (BSRF), Institute of High Energy Physics. The photon energy of 4B9B beamline covers from 10 to 1000 eV with an energy resolution power

(E/ΔE) of about 1500. The endstation comprises of three ultrahigh vacuum (UHV) chambers, namely, the analysis chamber, the preparation chamber and the fast entry chamber. The analysis chamber is equipped with a VG Scienta R4000 electron energy analyzer with a base pressure of ~4×10^{-11} mbar. The Mo 3d, N 1s and C 1s spectra were recorded using the photon energy of 500 eV and the O 1s was recorded at the photon energy of 700 eV. Binding energies (BE) of these core levels were calibrated with respect to the Au $4f_{7/2}$ (BE = 84 eV) feature from a clean gold foil that attached to the manipulator. All the data were recorded in UHV at room temperature. The spectral fitting was performed using the XPSPeak 4.1 software with Gaussian–Lorentzian functions after subtracting a Shirley background.

The NEXAFS measurements were carried out in total electron yield (TEY) mode at the Wide-Range beamline (BL24A) of National Synchrotron Radiation Research Center (NSRRC) in Hsinchu, Taiwan. All NEXAFS spectra (O K-edge and Fe L-edge XAS spectra) were normalized to the incident photon intensity monitored by the gold net that mounted after the rear mirror of the beamline. Then a linear non-resonance background was subtracted and an edge-jump of one was taken for the spectral tail (at ~40 eV higher than the adsorption edge) intensity relative to the pre-edge. The incident angle of X-ray was 90 °with respect to the substrate surface. The morphology of the MoO_3 film was acquired by the atomic force microscopy (AFM, DI Innova) operating in tapping mode. The image size was 3 μm × 3μm.

Results and discussion

Firstly, the evolution of the bare MoO_3 film under the thermal annealing from room temperature to 450 ℃ is studied. Fig. 1a shows the series of Mo 3d XPS spectra of the MoO_3 film at different temperatures. The spectra were fitted using several components in order to calculate the concentration of the reduced Mo ion species. To allow for the intensity calculations, each spectrum was normalized to the $3d_{5/2}$ peak of Mo^{6+}. The parameters of the fittings are present in the Supporting Information (ESI Table S1). For the as-deposited MoO_3 film, the dominant Mo $3d_{3/2}$ and $3d_{5/2}$ peaks appear to be symmetric and can be well fitted with one component locating at 235.6 eV and 232.5 eV, respectively, indicative of the presence of Mo^{6+} species[11, 25, 26]. With the annealing temperature increasing, the Mo 3d profiles change pronouncedly with the emergence of broad shoulders at the lower BE side of the Mo^{6+}, suggesting a partial reduction of the MoO_3 film. A well resolved peak is observed at the BE of 229.2 eV after annealing at 300 ℃, which is assigned to Mo^{4+} species[11]. This peak intensifies gradually when further increasing the annealing temperature. Also, the amount of Mo^{4+} species among total Mo species is found to increase accordingly till 400 ℃ as shown in Fig. 1b. While after annealed at 450 ℃, the concentration of Mo^{4+} species is stabilized. This suggests that the thermal reduction of MoO_3 film saturates at the temperature of ~ 400 ℃. Based on this result the FePc adsorbed samples were annealed within 400 ℃ in subsequent experiments. The partially reduced MoO_3 is denoted as MoO_x in this work, where $x < 3$. In addition, the morphology of the MoO_3 film before and after the thermal annealing at 400 ℃ is also shown in Fig. 2a and 2b, respectively. It is seen that the average size of the particles is roughly estimated to be

~ 100 nm for the MoO_3 film and ~ 30 nm for the MoO_x film. The MoO_3 film appears an average grain size with a root mean square (RMS) roughness of 2.5 nm, while the roughness of the MoO_x film is 1.2 nm. As a result, the MoO_x film would expect to have larger specific surface and supply more sites for FePc adsorption. And the subsequent adsorption of FePc on this MoO_x is found to have less influence on its morphology, as seen in Fig. S1 of the ESI.

Fig. 3a and 3b show the Mo 3d XPS spectra for the bare and 1 ML FePc covered MoO_x (3nm) films on the ITO substrates, respectively. Both spectra were fitted by four components corresponding to Mo^{6+} (232.6 eV), Mo^{m+} (231.3 eV), Mo^{n+} (230.4 eV) and Mo^{4+} (229 eV), respectively, according to previous work[11, 27]. Mo^{m+} and Mo^{n+} are two intermediate reduced species with valence state values in a sequence of $6 > m > n > 4$. The value of spin-orbit splitting for Mo 3d is ~ 3.1 eV and is allowed to vary within a small range during the fitting[27]. The final fitting results and parameters are listed in Table 1.

For the bare MoO_x film, the annealing leads to an obvious reduction of the Mo^{6+} into several species of lower chemical states. The portion of Mo^{4+} among the total Mo ions is about 19.5%. Whereas for the 1 ML FePc covered MoO_x sample, the reduction of Mo^{6+} appears higher under the same annealing temperature. The concentration of Mo^{4+} species is increased to 27.8%. The much higher yielding of Mo^{4+} ions implies that the FePc adsorption promotes the thermal reduction of the MoO_3. Besides the oxygen loss of MoO_3 in the annealing process, there should exist an additional

reaction channel involving direct interactions between FePc molecules and the MoO_3 substrate.

In order to verify the strong interactions at the FePc/MoO_x interface, the C 1s, N 1s and O 1s XPS as well as the O K-edge and Fe L-edge NEXAFS spectra were recorded for both multilayer and monolayer of FePc film covered samples. The C 1s shown in Fig. 4 demonstrates obvious differences under the two thicknesses of FePc on MoO_x. The C 1s of the multilayer film includes three main spectral features and can be deconvoluted with four components. The dominant peak at the BE of 284.8 eV (FWHM=0.9 eV) can be ascribed to the contributions of benzene carbon atoms and the peak at 286 eV (FWHM=0.9 eV) is from the pyrrole carbon atoms according to previous reports[28]. In addition, two peaks exist at the higher BE of 286.8 and 288.0 eV, corresponding to the shake-up satellites from the benzene-type carbons and pyrrole-type carbons, respectively.[28] In contrast, the C 1s spectrum of the 1 ML FePc film is comprised of two features and weaker satellite peaks. The main peak at 286.0 eV (FWHM=1.1 eV), corresponding to the benzene carbon, shifts to the higher BE with a value of 1.2 eV with respect to the multilayer film. The peak at 287.2 eV (FWHM = 1.2 eV) is associated with the pyrrole-type carbons. Furthermore, the N 1s core level also shifts to the higher BE with a value of ~1.0 eV for the 1 ML FePc film relative to the multilayer film (see Fig. S2 in ESI). This rigid shift of C 1s and N 1s core levels to higher BE agrees well with previous reports regarding on the FePc adsorption on TiO_2 surface[29], suggesting a strong interaction at the FePc/MoO_x interface. For FePc adsorption on TiO_2 (110) surface, the first FePc monolayer was

oxidized, and both occupied and unoccupied electronic structures were changed, leading to the quenching of the HOMO-LUMO shakeup transitions in the C 1s and N 1s core level spectra. In this work, the shake-up satellites are also observed to diminish clearly in the 1 ML FePc/MoO_x sample, implying the excitation channel is blocked or strongly reduced due to the strong electronic coupling between the FePc molecules and the MoO_x substrate[29].

Likewise, the O 1s XPS spectra for the 1 ML FePc/MoO_x and the bare MoO_x samples are compared as shown in the Fig. 5. Due to the limited energy resolution, it is only seen a broad feature for both spectra regardless of a difference on the peak intensity. Since there is no oxygen in FePc molecules, the O 1s spectra can be decomposed into several species that bond to different Mo ions with different chemical states as shown in Fig. 5. The fitting parameters are present in the Table S2 of the ESI. It is seen that the O 1s spectrum of the bare MoO_x substrate can be well fitted by three oxygen components at the BE of 530.2, 530.8 and 531.6 eV, which correspond to the oxygen species bonding to Mo ions in different chemical states of +6, immediate and +4, respectively. From the peak fitting, the relative amount of each oxygen species is 42.4%, 36.1% and 21.5%, respectively, in agreement with the calculations of each Mo ion from Mo 3d data in Fig. 3. While for the fitting of the O 1s spectrum of the 1 ML FePc/MoO_x sample, besides the above three components, an additional component at 532.3 eV is needed to well reproduce the spectrum envelop. In this way, the concentration of oxygen species at 530.2 eV in FePc/MoO_x sample attenuates to 19% and the oxygen species at 530.7 eV and 531.6 eV increase to 48%

and 33.8%, respectively. The variations of these three oxygen species at lower BE are comparable with the tendency of the Mo ions after the 1 ML FePc deposited. The concentration of the new oxygen species that appears at 532.3 eV is about 9.2%. This oxygen species suggests the presence of a new type of oxygen species at the FePc/MoO_x interface. Since no Mo species with chemical states lower than +4 are detected, we assign tentatively this new oxygen species to the terminal oxygen that coupled with the FePc molecules.

Fig. 6 displays the O K-edge NEXAFS spectra for MoO_3, MoO_x, and 1 ML FePc adsorbed MoO_x samples. The resonances at O K-edge are extremely sensitive to the electronic structure and chemical environment of O atoms[30]. For the stoichiometric MoO_3, six features at least are recognized, and are labeled as A-F. The resonances at the energy range of 529-538 eV are assigned to the transitions from the O 1s level to the 2p-4d hybridized orbitals. Due to the crystal field splitting of MoO_6 octahedron field and the spin exchange effect, these resonances split into two dominant peaks at 530.8 eV with t_{2g} symmetry (A) and 533.8 eV with e_g symmetry (C)[31-33]. The energy difference between A and C is ~ 3 eV, in good agreement with previous work[32, 34]. Features of E at 539.3 eV and F at 543.8 eV are assigned to the transitions from O 1s level to the O 2p-Mo 5s and O 2p-Mo 5p hybrid orbitals, respectively. Whereas, the intensity of peak A of the MoO_x film decreases slightly with respect to the MoO_3 film. According to the calculations of O K-edge NEXAFS spectra of MoO_3[34], peak A is mainly contributed by the terminal oxygen and the asymmetrical bridging oxygen species, while peak C is originated from the terminal oxygen and the symmetric

bridging oxygen. The arrangement of these oxygen atoms is schematically shown in Fig. 8. The reduction of peak A may be explained as following. After annealed at 400 ℃, the MoO_x film is reduced with a considerable amount of oxygen vacancies yielding in the film. The production of oxygen vacancies leads to the partial filling of the Mo 4d by the remaining electrons at the defects, thus inducing decreased density of states of the unoccupied Mo 4d orbitals[18]. Therefore the hybridization of O 2p with the decayed Mo 4d unoccupied orbitals would expect to give rise to lower NEXAFS intensities. Certainly, the oxygen loss of the annealed film also contributes the decrease of the O K-edge.

For the 1 ML FePc covered MoO_x sample, the intensity of peak A further declines, suggesting a heavier reduction of MoO_x with FePc adsorption than the bare MoO_x sample. This result agrees well with the Mo 3d XPS analysis. Simultaneously, the energy separation between the t_{2g} and e_g is observed to enhance by a value of ~0.6 eV with respect to that of both MoO_x and MoO_3 samples. It is known that the energy splitting between t_{2g} and e_g is mainly determined by the strength of the crystal field[35]. Therefore, the incremental separation of the O doublets may suggest a variation of the coordination field around oxygen atoms at the FePc/MoO_x interface. For metal phthalocyanine and porphyrin molecules adsorption on TMO surface, it has been revealed that the molecules anchor on the surface via the combination of the core metallic atoms with the surface terminated oxygen. For instance, Szymon *et al.* have demonstrated CuPc molecules adsorbing on TiO_2 (011)-(2×1) surface arranged along the outstanding rows of oxygen atoms with central Cu atoms located over oxygen

rows[36, 37]. Recently, Wang *et al.* observed that the NiTPP molecules prefer to assemble with center Ni atoms above the top bridging O rows of the rutile TiO_2 (110) surface[38]. Therefore, we suggest here the adsorbed FePc molecules bond to the surface through a direct coordination of Fe with the outstanding terminal oxygen of MoO_x.

The Fe-O bonding may be evidenced by the Fe L-edge data that are shown in Fig. 7. The spectra are dominated by two groups of peaks, marked as L_3 and L_2 which are originated from the electronic transitions from the Fe $2p_{3/2}$ and $2p_{1/2}$ levels to the Fe 3d orbital, respectively. For the L_3 resonance, it is roughly resolved with A (~705.8 eV) and B (~708.0 eV) sub-bands. It can be also seen that the intensity of A sub-band weakens more pronouncedly than B at the interface. The shape of Fe L-edge is known to be fundamentally dependent on the multiplet effects[39] and the polarization effects. The latter factor can be ruled out because the FePc film deposited on the MoO_x substrate appears polymorphous and lack of uniform molecular orientation (see the angle dependence of C K-edge for the multilayer of FePc film in Fig. S3 of ESI). In a recent work, the resonance A of the FePc molecule was ascribed to the d orbitals mainly with out-of plane symmetry such as d_{z2} orbital, while resonance B consists of d orbitals with both in-plane and out-of plane symmetries[39,40]. Therefore, the relative fast decrease of A sub-band could be associated with the electronic coupling between the Fe ion and the terminal oxygen along the z axial of the molecule. It might result in a coordination of Fe-O bonding where the oxygen provides an electron pair and the Fe supplies unoccupied d orbitals. This interaction nature is consolidated by the ~0.7 eV shift of Fe 2p core level to the higher BE in the monolayer film with respect to the

multilayer film (Fig. S4 in ESI). The higher BE of Fe 2p core level for the 1 ML FePc film suggests a partial oxidation of the Fe ion, in agreement to the augment of coordination number of the Fe ion[41]. This coordination of central Fe of FePc with extra oxygen have been widely demonstrated to play crucial role for the oxygen reduction reaction (ORR) in which the FeN_4 structures including the phthalocyanine and porphrine molecules are regarded as the active site for oxygen adsorption[42,43].

Overall, core levels of C 1s, N 1s and Fe 2p of the FePc molecules have shown unanimously to shift toward higher BE, suggesting an oxidation of the FePc molecules at the FePc/MoO_x interface. Except for the loss of the lattice oxygen during the thermal annealing, the interaction between the FePc and the MoO_x accounts for the improved reduction of the substrate covered with FePc. The oxidation of FePc and the reduction of the MoO_x substrate suggest a charge transfer from the FePc molecule to the substrate. From the inorganic semiconductor theory point of view, the charge transfer from molecules towards the substrate suggests a p-type doping to the molecules, thus should cause a rigid shift of core levels of the molecules to lower BE. This is opposite to what we measured in the XPS data. In fact, the energy band theory or doping theory model that developed from the inorganic crystalline matter should be applied cautiously in organic systems due to the localization of the electronic wave functions and the resulting strong correlation effects between the electrons and the nuclei in organics[44,45]. In particular, the 1 ML FePc film on the MoO_x in this work shows to be highly disorder, and the molecule-substrate interaction seems much stronger than the molecule-molecule interaction. In this way, the charge transfer is

believed to be rather localized at the molecules and the band theory is not applicable any more. Therefore, the charge transfer from the molecule to the substrate would arouse the decrease of the electron density around the Pc ring and thus the BEs of C 1s, N 1s and Fe 2p core levels increase at the interface. It is also noticed that the shift value of each core level is different, indicative of a site dependence on the molecule for the interaction with the MoO_x. The relative small shift (0.7 eV) for the Fe 2p core level may be reconciled by the back donation of the electrons from the terminal oxygen of the substrate to the central Fe ion of the FePc molecule. Such bidirectional charge transfer process was also discussed recently for several phthalocyanines on metal supports[46-48]. In the other hand, the O 1s and Mo 3d core levels of the MoO_x substrate show a negligible energy shift (Fig. 3 and Fig. 5) during the interface formation. The fixing of the core levels of the MoO_x substrate may be due to the pinning of the Fermi level at the band gap where Mo 4d derived band gap states have been revealed for the reduced MoO_3[12]. Finally, the O K-edge and the Fe L-edge NEXAFS data unanimously support a strong interaction involving a Fe-O coordination at the FePc/MoO_x interface. A tentative adsorption model for a monolayer FePc molecules adsorbed on MoO_x is schematically shown in Fig. 7. The MoO_3 bilayer structure is referred from literatures[27,34]. In this adsorption model, the center of the FePc molecule locates above the terminal O string, facilitating the local bonding between the terminal O and the Fe (II) center. This local bridging via Fe-O coordination may facilitate the charge transfer from FePc molecules to the MoO_x substrate.

Conclusions

In this work, the interaction at the FePc/MoO_x interface was investigated using the SRPES and NEXAFS spectroscopies at room temperature. The monolayer FePc covered MoO_x sample was obtained from the annealing of FePc multilayer deposited MoO_3 sample at 400 ℃. Compared with the bare MoO_3 film, the FePc adsorption is found to improve the thermal reduction of the MoO_3 substrate. Regardless of the loss of lattice oxygen, this effect is associated with the extra chemical reactions between FePc and MoO_x at the interface. Simultaneously, a partial oxidation of the FePc molecules at the interface is revealed. A strong electronic coupling, involved with a direct Fe-O coordination and an electron transfer from the phthalocyanine ring toward the substrate, is suggested for FePc adsorption on MoO_x after a thermal annealing. This Fe-O coupling at FePc/MoO_3 interface may supply a straightforward channel for the fast charge transfer from the FePc adlayer to the MoO_3.

Acknowledgements

The authors gratefully acknowledge the financial support from the National Natural Science Foundation of China (Grant Nos. 11175172, 11175183, 10975138 and U1232137) and the Fundamental Research Funds for the Central Universities (Grant No. WK2310000011). We also thank very much the students of BSRF and NSRRC for their kind helps during the synchrotron radiation experiments.

References

1 M. Kröger, S. Hamwi, J. Meyer, T. Riedl, W. Kowalsky and A. Kahn, *Appl. Phys. Lett.*, 2009, **95** , 123301.

2 S. Hamwi, J. Meyer, M. Kröger, T. Winkler, M. Witte, T. Riedl, A. Kahn and W. Kowalsky, *Adv. Funct. Mate.*, 2010, **20**, 1762-1766.

3 C. Y. H. Chan, C. M. Chow and S. K. So, *Org. Electron.*, 2011, **12**, 1454-1458.

4 Y. H. Kim, S. Kwon, J. H. Lee, S. M. Park, Y. M. Lee and J. W. Kim, *J. Phys. Chem. C*, 2011, **115**, 6599-6604.

5 M. Vasilopoulou, G. Papadimitropoulos, L. C. Palilis, D. G. Georgiadou, P. Argitis, S. Kennou, I. Kostis, N. Vourdas, N. A. Stathopoulos and D. Davazoglou, *Org. Electron.*, 2012, **13**, 796-806.

6 B. Minaev, G. Baryshnikov and H. Agren, *Phys. Chem. Chem. Phys.*, 2014, **16**, 1719-1758.

7 J. Schnadt, J. N. O'Shea, L. Patthey, L. Kjeldgaard, J. Åhlund, K. Nilson, J. Schiessling, J. Krempaský, M. Shi, O. Karis, C. Glover, H. Siegbahn, N. Mårtensson and P. A. Brühwiler, *J. Chem. Phys.*, 2003, **119**, 12462.

8 W. Chen, L. Wang, D. C. Qi, S. Chen, X. Y. Gao and A. T. S. Wee, *Appl. Phys. Lett.*, 2006, **88**, 184102.

9 A. Fang and M. Haataja, *Phys. Rev. E*, 2014, **89**, 022407.

10 A. Soultati, D. G. Georgiadou, A. Douvas, P. Argitis, D. Alexandropoulos, N. A. Vainos, N. A. Stathopoulos, G. Papadimitropoulos, D. Davazoglou and M. Vasilopoulou, *Microelectron. Eng.*, 2014, **117**, 13-17.

11 M. T. Greiner, M. G. Helander, Z. B. Wang, W. M. Tang, J. Qiu and Z. H. Lu, *Appl. Phys. Lett.*, 2010, **96**, 213302.

12 L. Y. Liu, L. Wan, L. Cao, Y. Y. Han, W. H. Zhang, T. X. Chen, P. P. Guo, K. Wang and F. Q. Xu, *Appl. Surf. Sci.*, 2013, **271**, 352-356.

13 Y. Sun, C. J. Takacs, S. R. Cowan, J. H. Seo, X. Gong, A. Roy and A. J. Heeger, *Adv. Mater.*, 2011, **23**, 2226-2230.

14 W. Zhang, L. Cao, L. Wan, L. Liu and F. Xu, *J. Phys. Chem. C*, 2013, **117**, 21351-21358.

15 H. Ishii, K. Sugiyama, E. Ito and K. Seki, *Adv. Mater.*, 1999, **11**, 605-625.

16 J. –C., Dupin, D. Gonbeau, P. Vinatier and A. Levasseur, *Phys. Chem. Chem. Phys.*, 2000, **2**, 1319-1324.

17 S. Braun, W. R. Salaneck and M. Fahlman, *Adv. Mater.*, 2009, **21**, 1450-1472.

18 J. G. Chen, *Surf. Sci. Rep.*, 1997, **30**, 1-152.

19 M. S. Roy, M. Kumar, P. Jaiswal and G. D. Sharma, *Radiat. Meas.*, 2004, **38**, 205-209.

20 R. W. I. de Boer, A. F. Stassen, M. F. Craciun, C. L. Mulder, A. Molinari, S. Rogge and A. F. Morpurgo, *Appl. Phys. Lett.*, 2005, **86**, 262109.

21 G. D. Sharma, R. Kumar and M. S. Roy, *Sol. Energy Mat. Sol. C.*, 2006, **90**, 32-45.

22 J. H. Shu, H. C. Wikle and B. A. Chin, *Sensor. Actuat. B-Chem.*, 2010, **148**, 498-503.

23 P. S. Johnson, P. L. Cook, I. Zegkinoglou, J. M. Garcia-Lastra, A. Rubio, R. E.

Ruther, R. J. Hamers and F. J. Himpsel, *J. Chem. Phys.*, 2013, **138**, 044709.
24 P. S. Johnson, J. M. Garcia-Lastra, C. K. Kennedy, N. J. Jersett, I. Boukahil, F. J. Himpsel and P. L. Cook, *J. Chem. Phys.*, 2014, **140**, 114706.
25 V. Bhosle, A. Tiwari and J. Narayan, *J. Appl. Phys.*, 2005, **97**, 083539.
26 W. -C. Chang, X. Qi, J. -C. Kuo, S. -C. Lee, S. -K. Ng and D. Chen, *Crystengcomm*, 2011, **13**, 5125.
27 D. O. Scanlon, G. W. Watson, D. J. Payne, G. R. Atkinson, R. G. Egdell and D. S. L. Law, *J. Phys. Chem. C*, 2013, **114**, 4636-4645.
28 M. -N. Shariati, J. Lüder, I. Bidermane, S. Ahmadi, E. Göthelid, P. Palmgren, B. Sanyal, O. Eriksson, M. N. Piancastelli, B. Brena and C. Puglia, *J. Phys. Chem. C*, 2013, **117**, 7018-7025.
29 P. Palmgren, K. Nilson, S. Yu, F. Hennies, T. Angot, C. I. Nlebedim, J. –M. Layet, G. Le Lay and M. Gothelid, *J. Phys. Chem. C*, 2008, **112**, 5972-5977.
30 W. Zhang, K. Wang, L. Fan, L. Liu, P. Guo, C. Zou, J. Wang, H. Qian, K. Ibrahim, W. Yan, F. Xu and Z. Wu, *J. Phys. Chem. C*, 2014, **118**, 12837-12844.
31 M. Sing, R. Neudert, H. von Lips, M. S. Golden, M. Knupfer and J. Fink, *Phys. Rev. B*, 1999, **60**, 8559-8568.
32 G. Wu, T. Sekiguchi, Y. Baba and I. Shimoyama, *Nulear. Instru. Math. Phys. Res. B*, 2006, **245**, 406-410.
33 H. M. Tsai, K. Asokan, C. W. Pao, J. W. Chiou, C. H. Du, W. F. Pong, M. H. Tsai and L. Y. Jang, *Appl. Phys. Lett.*, 2007, **91**, 022109.
34 M. Cavalleri, K. Hermann, S. Guimond, Y. Romanyshyn, H. Kuhlenbeck and H. J. Freund, *Catal. Today*, 2007, **124**, 21-27.
35 J. Crocombette, M. Pollak, F. Jollet, N. Thromat and M. Gautier-Soyer, *Phys. Rev. B*, 1995, **52**, 3143-3150.
36 S. Godlewski, A. Tekiel, J. S. Prauzner-Bechcicki, J. Budzioch and M. Szymonski, *Chemphyschem*, 2010, **11**, 1863-1866.
37 S. Godlewski, A. Tekiel, J. S. Prauzner-Bechcicki, J. Budzioch, A. Gourdon and M. Szymonski, *J. Chem. Phys.*, 2011, **134**, 224701.
38 C. Wang, Q. Fan, S. Hu, H. Ju, X. Feng, Y. Han, H. Pan, J. Zhu and J. M. Gottfried, *Chem. Commun.*, 2014, **50**, 8291-8294.
39 F. Petraki, H. Peisert, U. Aygül, F. Latteyer, J. Uihlein, A. Vollmer and T. Chassé, *J. Phys. Chem. C* 2012, **116**, 11110 −11116.
40 P. S. Johnson, J. M. Garcí a-Lastra, C. K. Kennedy, N. J. Jersett, I. Boukahil, F. J. Himpsel and P. L. Cook, *J. Chem. Phys.*, 2014, **140**, 114706.
41 R. Cao, R. Thapa, H. Kim, X. Xu, M. G. Kim, Q. Li, N. Park, M. Liu and J. Cho, *Nat. Commun.*, 2013, **4**, 1-7.
42 M. Nagasaka, H. Yuzawa, T. Horigome, A. P. Hitchcock and N. Kosugi, *J. Phys. Chem. C*, 2013, **117**, 16343-16348.
43 S. Kattel and G. Wang, *J. Phys. Chem. Lett.* 2014, **5**, 452 −456.
44 S. Braun, W. R. Salaneck and M. Fahlman, *Adv. Mate.*, 2009, **21**, 1450-1472.
45 H. Ishii, K. Sugiyama, E. Ito and K. Seki, *Adv. Mate.*, 1999, **11**, 605-625.
46 L. Romaner, G. Heimel, J.-L. Brédas, A. Gerlach, F. Schreiber, R. L. Johnson, J. Zegenhagen, S. Duhm, N. Koch and E. Zojer, *Phys. Rev. Lett.* 2007, **99**,

256801.
47 S. Lindner, U. Treske and M. Knupfer, *Appl. Surf. Sci.*, 2013, **267**, 62-65.
48 F. Petraki, H. Peisert, J. Uihlein, U. Aygül and T. Chassé, *Beilstein J. Nanotechnol.*, 2014, **5**, 524-531.

Figures

Fig. 1

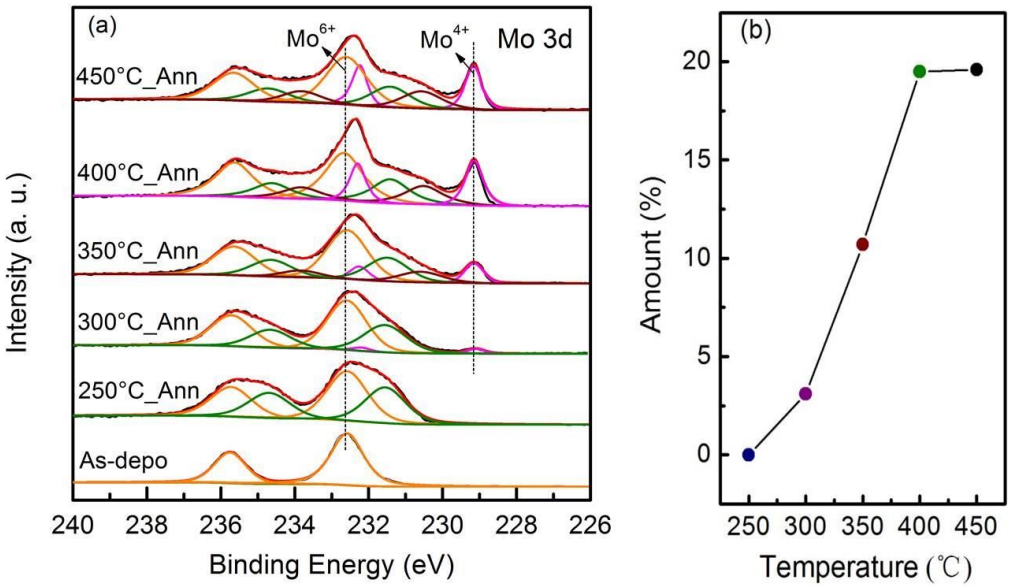

Fig. 1 Mo 3d XPS spectra of MoO_3 film (a) and the portion of Mo^{4+} species in the MoO_3 film (b) as a function of annealing temperature.

Fig. 2

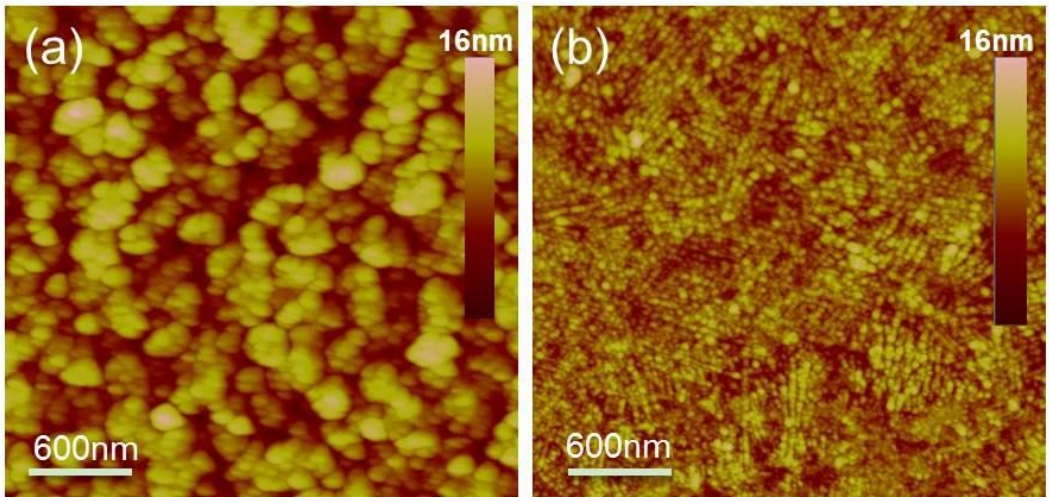

Fig. 2 The AFM images of MoO_3 film (a) and MoO_x film (b) that was annealed at 400 ℃.

Fig. 3

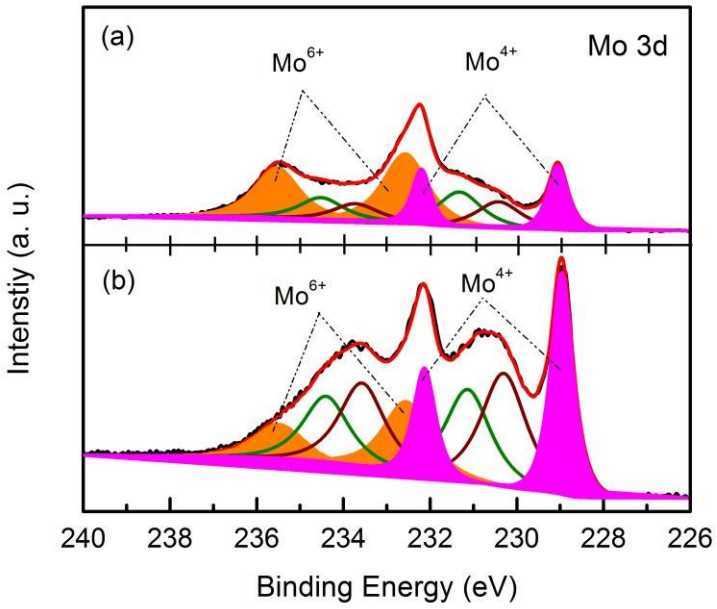

Fig. 3 Mo 3d XPS spectra of (a) bare MoO_x and of (b) MoO_x adsorbed with one ML FePc.

Fig. 4

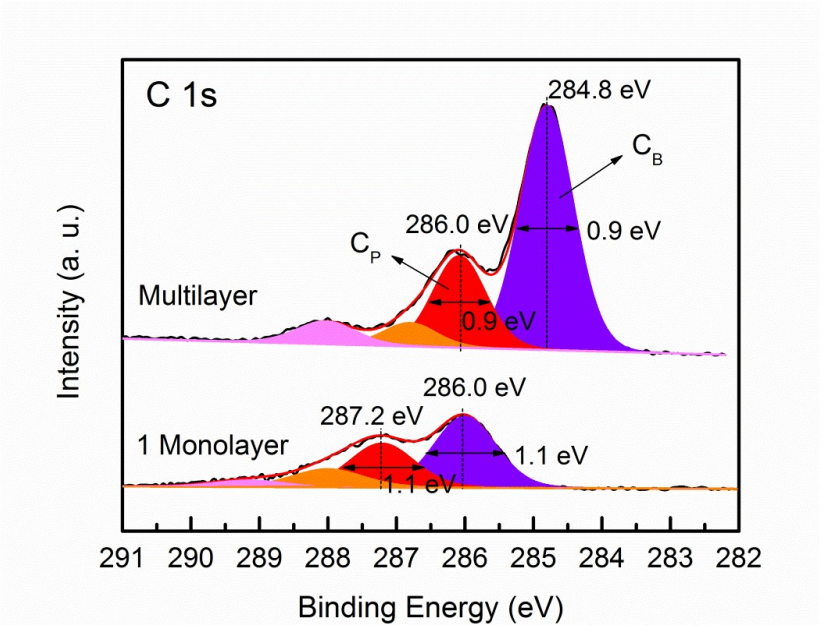

Fig. 4 C 1s XPS spectra of the multilayer (top) and monolayer (bottom) FePc films adsorbed on MoO_x. The FWHMs of the C_B and C_P species for the multilayer FePc are both 0.9 eV, and for the one monolayer FePc are both 1.1 eV. The G-L% are fixed as 20% during the fitting process.

Fig. 5

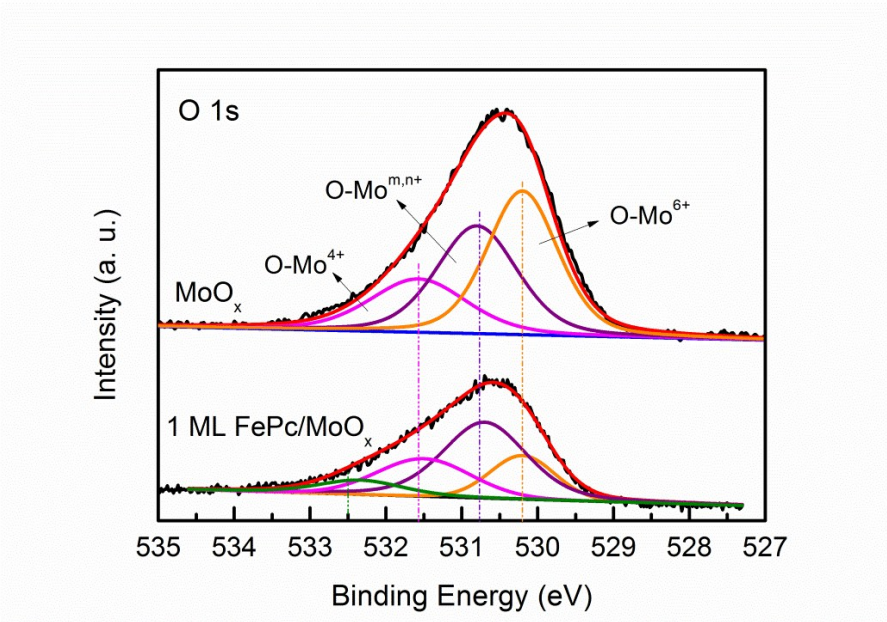

Fig. 5 O 1s XPS spectra of bare MoOx (top) and of MoOx adsorbed with one ML FePc (bottom).

Fig. 6

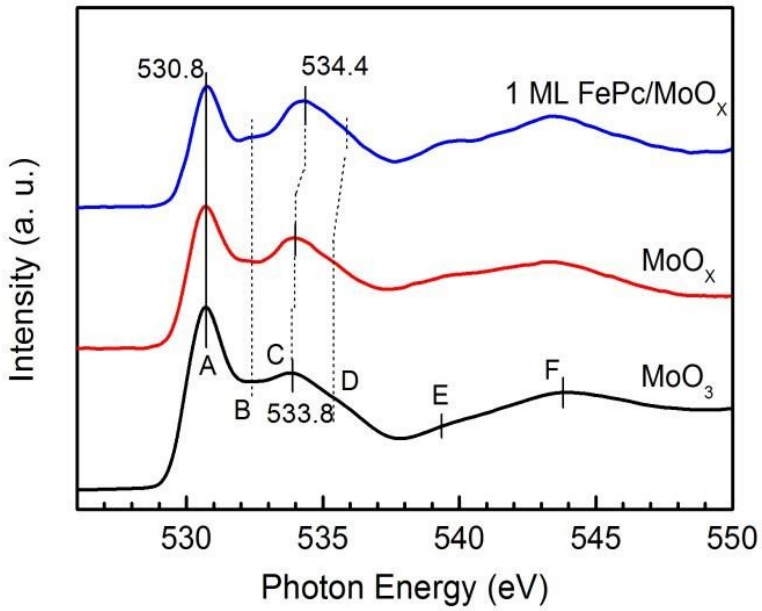

Fig. 6 O K-edge XAS spectra of MoO_3, MoO_x, and 1 ML FePc/MoO_x with the x-ray incident angle of 90 °with respect to the substrate surface plane.

Fig. 7

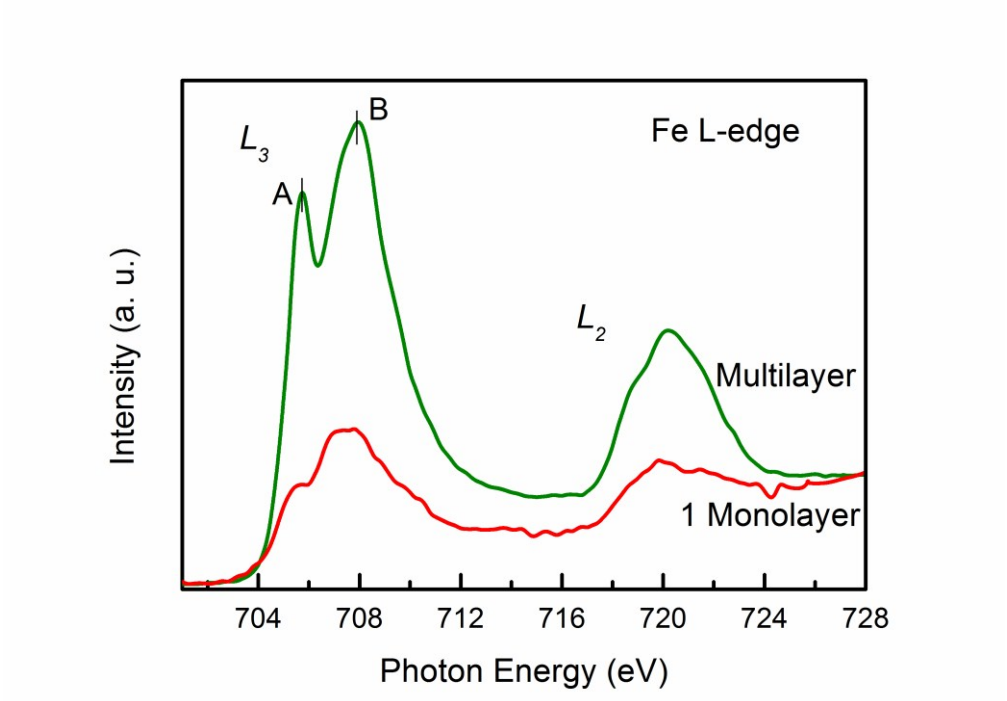

Fig. 7 Fe L-edge XAS spectra of Fe ions in multilayer and a monolayer FePc with the x-ray incident angle of 90 °with respect to the substrate surface plane.

Fig. 8

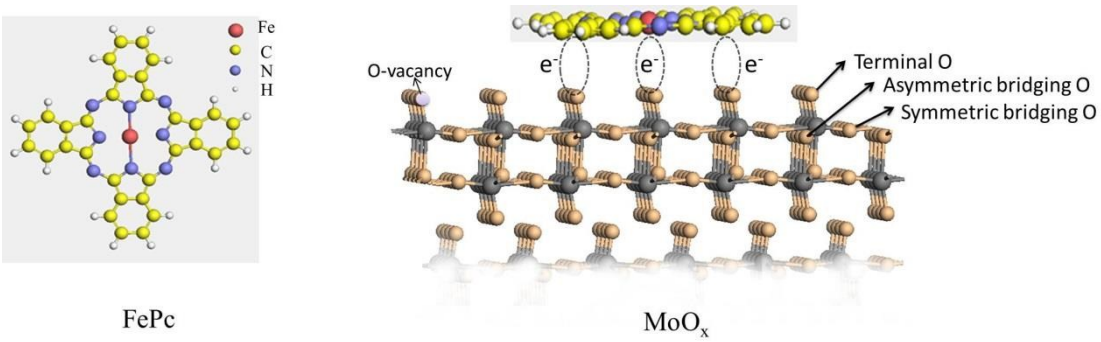

Fig. 8 The molecular structure of FePc (left), and schematic diagram for the adsorption configuration of FePc on MoO_x (right).

Table

Table 1

Mo species			E_B (eV)	Intensity	FWHM（eV）	Amount
(a)	+6	$3d_{3/2}$	235.5	150	1.20	43.7%
		$3d_{5/2}$	232.6	208	1.20	
	+m	$3d_{3/2}$	234.5	65	1.20	20.8%
		$3d_{5/2}$	231.3	105	1.20	
	+n	$3d_{3/2}$	233.7	50	1.20	15.9%
		$3d_{5/2}$	230.4	80	1.20	
	+4	$3d_{3/2}$	232.2	70	0.50	19.5%
		$3d_{5/2}$	229.0	90	0.55	
(b)	+6	$3d_{3/2}$	235.5	50	1.25	17.8%
		$3d_{5/2}$	232.6	80	1.23	
	+m	$3d_{3/2}$	234.5	75	1.23	25.6%
		$3d_{5/2}$	231.3	112	1.23	
	+n	$3d_{3/2}$	233.7	83	1.23	28.8%
		$3d_{5/2}$	230.4	127	1.23	
	+4	$3d_{3/2}$	232.2	73	0.60	27.8%
		$3d_{5/2}$	229.0	130	0.60	

Table 1. Mo 3d XPS peak fitting results including BE (E_B), peak area (Area), full width at half maximum (FWHM) and the amount of each component peak of Mo species, for both bare MoO_x and 1 ML FePc adsorbed MoO_x.

Note: Symbol (a) and (b) in the table stand for the fitting results of Fig. 2a, and 2b.

"+m" and "+n" are for the medium states of Mo ions between +6 and +4 valence states. The Lorentz-Gaussian (GL%) is 20% during the fitting process.